Structure and Magnetic Properties of Glycine Radical in Aqueous Solution at Different pH Values

Nadia Rega, Maurizio Cossi, and Vincenzo Barone*

Contribution from the Dipartimento di Chimica, Università Federico II via Mezzocannone 4, I-80134 Napoli, Italy

Received December 15, 1997. Revised Manuscript Received March 26, 1998

Abstract: A recently developed quantum mechanical approach devoted to the study of unstable species in solution was applied to the radicals resulting from the homolytic breaking of the $C^{\alpha}-H^{\alpha}$ bond of glycine in aqueous solution at different pH values.The computational protocol includes density functional calculations, simulation of the solvent by a mixed discrete-continuum approach, and averaging of spectroscopic properties over the most important vibrational motions. In vacuo computations provide reliable results for the zwitterionic form when using hybrid Hartree−Fock/density-functional methods with purposely tailored basis sets. Under the same conditions, disappointing results are obtained for the magnetic properties of neutral and, especially, anionic forms. Although the modifications of the structure and the magnetic properties of these species induced by the solvent are well reproduced by either a continuum model or a supermolecule approach, quantitative results can be obtained only by a mixed discrete-continuum model. Vibrational averaging effects further improve the results, leading to remarkable agreement between computed and experimental hyperfine coupling constants. Together with its numerical accuracy, the interest of the proposed approach is that it can be routinely applied to large systems also by nonspecialists and that it allows a straightforward interpretation of the results in terms of different intrinsic and environmental effects.

1. Introduction

Many biochemical reactions involve amino acid radicals.[1] For instance, there is strong evidence that free radicals are intermediates in penicillin and cephalosphorin biosynthesis[2,3] and in the bioconversion of cyclopropylglycine to ethylene during the maturation of fruits.[4] Furthermore, oxidative damage to biological material, of importance in pharmacology, toxicology, and radiation biology,[5,6] frequently proceeds through this kind of radicals.

The aliphatic radicals that are peculiar to amino acids and their derivatives are α-carbon-centered radicals.[7] When the amino group is present in the free-base form, there is extensive delocalization of the unpaired spin density and an increased stability of the radical through the synergic action of the electron-withdrawing (capto) carboxyl group and of the electron-donating (dative) aminic moiety. However, this so-called captodative effect[7] is lost when the amino group is protonated, thus strongly modifying the characteristics of protomeric radical species with respect to the parent amino acids. Therefore, a better knowledge of the structural, thermodynamic, and spectroscopic characteristics of amino acid radicals in aqueous solution could have a significant impact in different areas. This has stimulated several groups to investigate the radicals derived from the simplest amino acid (glycine) by both theoretical[8−13] and experimental[14−17] approaches.

From an experimental point of view, a number of convincing, albeit indirect, evidences indicate that, contrary to the parent molecule, in aqueous solution the glycine radical prefers a neutral structure (i.e., $NH_2CHCOOH$ in place of $NH_3^+CHCOO^-$), which prevails over the cationic form ($NH_3^+CHCOOH$) even at pH = 1.[14−16] On the other hand, the anion radical (NH_2CHCOO^-) becomes the dominant species above pH = 10.[14−16] Also, the electron-spin resonance (ESR) spectra show some unexpected features. For instance, the isotropic hyperfine coupling constant (hcc) for the hydrogen atom directly bonded to the radical center (H^{α}) is anomalously low in the whole pH range (11.8 G below pH = 10 and 13.8 G above this value). This is to be contrasted with the more usual hcc of 26.8 G observed for H^{α} in the zwitterionic form present in the solid state.[17] At the same time, the hcc's of aminic hydrogens are strictly equivalent in acidic or neutral aqueous solutions (5.6

* To whom correspondence should be addressed. Tel.: +3981-5476503. Fax: +3981-5527771. E-mail:enzo@chemna.dichi.unina.it.

(1) Stuble, J. A. *Annu. Rev. Biochem.* **1989**, *58*, 257.
(2) Baldwin, J. E.; Bradley, M. *Chem. Rev.* **1990**, *90*, 1079.
(3) Baldwin, J. E.; Adlington, R. M.; Marquess, D. G.; Pitt, A. R.; Porter, M. J.; Russell, A. T. *Tetrahedron* **1996**, *52*, 2515; 2537.
(4) Baldwin, J. E.; Addlington, R. M.; Lajoie, G. A.; Lowe, C.; Baird, P. D.; Prout, K. *J. Chem. Soc., Chem. Commun.* **1988**, 775.
(5) Von Sonntag, C. *The Chemical Basis of Radiation Biology*; Taylor and Francis: New York, 1987.
(6) Stadtman, E. R. *Annu. Rev. Biochem.* **1993**, *62*, 797.
(7) Easton, C. J. *Chem. Rev.* **1997**, *97*, 53.
(8) Yu, D.; Rauk, A.; Armstrong, D. A. *J. Am. Chem. Soc.* **1995**, *117*, 1789.
(9) Rauk, A.; Yu, D.; Armstrong, D. A. *J. Am. Chem. Soc.* **1997**, *119*, 208.
(10) Barone, V.; Adamo, C.; Grand, A.; Brunel, Y.; Fontecave, M.; Subra, R. *J. Am. Chem. Soc.* **1995**, *117*, 1083.
(11) Barone, V.; Adamo, C.; Grand, A.; Subra, R. *Chem. Phys. Lett.* **1995**, *242*, 35.
(12) Barone, V.; Adamo, C.; Grand, A.; Jolibois, F.; Brunel, Y.; Subra, R. *J. Am. Chem. Soc.* **1995**, *117*, 12618.
(13) Barone, V.; Capecchi, G.; Brunel, Y.; Dheu Andries, M. L.; Subra, R. *J. Comput. Chem.* **1997**, *14*, 1720.
(14) Armstrong, D. A.; Rauk, A.; Yu, D. *J. Chem. Soc., Perkin Trans. 2* **1995**, 553.
(15) Paul, v. H.; Fischer, H. *Helv. Chim. Acta* **1971**, *54*, 485.
(16) Neta, P.; Fessenden, R. W. *J. Phys. Chem.* **1971**, *75*, 738.
(17) Ghosh, D. K.; Wiffen, D. H. *J. Chem. Soc.* **1960**, 1869.

S0002-7863(97)04232-7 CCC: $15.00
Published on Web 05/30/1998

G), but they become slightly different at basic pH (3.4 and 2.9 G). Once again, a very different situation is found in the solid state, where a single but very high hcc (16.6) is observed for the hydrogen atoms of the NH_3 moiety.

Unfortunately, interpretation of these data in structural terms is quite indirect since the measured quantities result from the superposition of different contributions that are very difficult, when not impossible, to separate. Under such circumstances, quantum mechanical computations can provide an invaluable support to experiment since they are able to evaluate separately the effect of different contributions. The only problem is that the computational models must be at the same time reliable and rapid enough to allow the study of sufficiently large systems. In this respect, most of the theoretical studies performed until now have not been completely satisfactory since they employ either isolated species or very crude solvent models. The limits of in vacuo computations are well illustrated by the fact that the zwitterionic form of glycine (and also of glycine radical, vide infra) is not even an energy minimum in the gas phase, whereas it becomes the most stable form in neutral aqueous solutions. In the same vein, too simplified solvent models often lead to unrealistic results.

In recent years, we have shown[18−21] that hybrid density functional/Hartree−Fock methods are quite promising in this connection when coupled to a proper treatment of averaging effects issuing from large amplitude vibrations. More recently, we have extended this computational protocol to condensed phases,[22−25] adding to the above features the self-consistent effect of a polarizable continuum mimicking the solvent. Since the first results of this new protocol were very promising, we decided to perform a comprehensive study of the species issuing from the homolytic breaking of the $C^{\alpha}-H^{\alpha}$ bond of glycine in aqueous solution at different pH values. The main purpose of the study is to analyze the equilibrium between neutral and zwitterionic forms both in vacuo and in aqueous solution and to characterize the anionic form prevalent at basic pH. From a more general point of view, through the description of this difficult system we would give a flavor of the potential impact of quantum-mechanical techniques in the characterization of unstable species involved in biological processes.

2. Theoretical Background

Electronic computations in vacuo were performed with the help of the Gaussian-94 package.[26] Stationary points (minima and saddle points) were located by full geometry optimizations, using quasi-Newton techniques[27] and characterized diagonalizing Hessian matrixes computed either analytically or by finite differences of analytical gradients.

Density functional calculations were carried out within the unrestricted Kohn−Sham (UKS) formalism using the Becke three-parameter model,[28] modified to include the LYP correlation functional[29] (B3LYP). On the basis of previous experience,[22,24] all the geometry optimizations have been performed with the standard 6-31+G(d,p) basis set.[30] Improved magnetic properties were obtained at the B3LYP level using the EPR-2 basis set, which was specifically optimized for this purpose.[20,22] Some test computations have been performed also at the MP2 level using the 6-31+G(d,p) basis set for geometry optimizations and the basis set purposely developed by Chipman[31] (hereafter referred to as CHIP) for evaluation of magnetic properties.

Isotropic hyperfine coupling constants a(X) are related to the spin densities at the corresponding nuclei by[32]

$$a(X) = \frac{8\pi}{3h} g_e \beta_e g_N \beta_N \sum_{\mu,\nu} \boldsymbol{P}^{\alpha-\beta}_{\mu,\nu} \langle \varphi_\mu | \delta(\boldsymbol{r}_K) | \varphi_\nu \rangle \qquad (1)$$

where β_e and β_N are the electron and nuclear magneton, respectively; g_e and g_N are the corresponding magnetogyric ratios, h is the Planck constant, $\delta(\boldsymbol{r}_K)$ is a Dirac delta operator, and $\boldsymbol{P}^{\alpha-\beta}$ is the difference between the density matrixes for electrons with α and β spin. In the present work, all the values are given in gauss (1 G = 0.1 mT), assuming that the free electron g value is appropriate also for the radicals. To convert data to MHz, one has to multiply them by 2.8025.

The study of large amplitude vibrations requires, especially in the case of relatively large molecules, some separation between the active large amplitude motion (LAM) and the *spectator* small amplitude modes (SAM). Once a suitable large-amplitude path (LAP) in mass-weighted Cartesian coordinates has been built (see next sections),[33,34] it can be parametrized in terms of its arc length s, referred to as the large amplitude coordinate (LAC).

When the couplings between different coordinates are negligible, the adiabatic Hamiltonian governing the effective one-dimensional motion assumes the simple form[35]

$$H(s,\boldsymbol{n}) = {}^1/_2 p_f^2 + V_{ad}(s,\boldsymbol{n}) \qquad (2)$$

where ${}^1/_2 p_f^2$ is the kinetic energy operator for motion along the LAP (fth degree of freedom), $\boldsymbol{n}$ is a vector containing the quantum numbers (supposed constant) for SAMs, and

$$V_{ad}(s,\boldsymbol{n}) = V_0(s) - V_0(s^0) + \eta \sum_{i=1}^{f-1} (n_i + {}^1/_2)(\omega_i(s) - \omega_i(s^0)) \qquad (3)$$

The $\omega_i(s)$'s are the harmonic frequencies of small amplitude vibrations as a function of the LAC, and s^0 refers to a suitable reference structure lying on the path. If the vibrational frequencies of SAMs do not vary along the path, the motion along the LSP is governed by the bare potential $V_0(s)$.

The vibrational states supported by this effective one-dimensional Hamiltonian can be found using the numerical

(18) Barone, V. *J. Chem. Phys.* **1994**, *101*, 6834; 10666.
(19) Barone, V. *Theor. Chim. Acta* **1995**, *91*, 113.
(20) Barone, V. *J. Phys. Chem.* **1995**, *99*, 11659.
(21) Barone, V. In *Recent Advances in Density Functional Methods*: Chong, D. P., Ed., World Scientific: Singapore, 1996; Part 1.
(22) Rega, N.; Cossi, M.; Barone, V. *J. Chem. Phys.* **1996**, *105*, 11060.
(23) Barone, V. *Chem. Phys. Lett.* **1996**, *262*, 201.
(24) Rega, N.; Cossi, M.; Barone, V. *J. Am. Chem. Soc.* **1997**, *119*, 12962.
(25) Jolibois, F.; Cadet, J.; Grand, A.; Rega, N.; Subra, R.; Barone, V. *J. Am. Chem. Soc.*, in press.
(26) Frisch, M. J.; Trucks, G. W.; Schlegel, H. B.; Gill, P. M. W.; Johnson, B. G.; Robb, M. A.; Cheeseman, J. R.; Keith, T. A.; Petersson, G. A.; Montgomery, J. A.; Raghavachari, K.; Al-Laham, M. A.; Zakrzewski, V. G.; Ortiz, J. V.; Foresman, J. B.; Cioslowski, J.; Stefanov, B. B.; Nanayakkara, A.; Challacombe, M.; Peng, C. Y.; Ayala, P. Y.; Chen, W.; Wong, M. W.; Andres, J. L.; Replogle, E. S.; Gomperts, R.; Martin, R. L.; Fox, D. J.; Binkley, J. S.; Defrees, D. J.; Baker, J.; Stewart, J. P.; Head-Gordon, M.; Gonzalez, C. Pople, J. A. GAUSSIAN 94, Gaussian. Inc., Pittsburgh, PA, 1995.
(27) Schlegel, H. B. In *Ab initio methods in Quantum Chemistry;* Lawley, K. P., Ed.; John Wiley & Sons: New York, 1987; p 249.
(28) Becke, A. D. *J. Chem. Phys.* **1993**, *98*, 5648.
(29) Lee, C.; Yang, W.; Parr, R. G. *Phys. Rev.* **1988**, *B37*, 785.
(30) Foresman, J. B.; Frisch, A. E. *Exploring Chemistry with Electronic Structure Methods*, 2nd ed.; Gaussian Inc.: Pittsburgh, PA, 1996.
(31) Chipman, D. M. *Theor. Chim. Acta* **1989**, *76*, 73; *J. Chem. Phys.* **1989**, *54*, 55.
(32) Weltner, W., Jr. *Magnetic Atoms and Molecules*; Van Nostrand: New York, 1983.
(33) Halgren, T. A.; Lipscomb, W. N. *Chem. Phys. Lett.* **1977**, *49*, 225.
(34) Zhixing, C. *Theor. Chim. Acta* **1989**, *75*, 481−483.
(35) Miller, W. H.; Handy, N. C. : Adams, J. E. *J. Chem. Phys.* **1980**, *72*, 99−112.

procedure described, e.g., in ref 36. Then, the expectation value $\langle O\rangle_T$ of a given observable at absolute temperature T is given by

$$\langle O\rangle_T = O_{\text{ref}} + \frac{\sum_{j=0}^{\infty}\langle j|\Delta O|j\rangle \exp[(\epsilon_0 - \epsilon_j)/KT]}{\sum_{j=0}^{\infty}\exp[(\epsilon_0 - \epsilon_j)/KT]} \qquad (4)$$

where O_{ref} is the value of the observable at the reference configuration, $\Delta O(s)$ is the expression (here a spline fit) giving its variation as a function of the progress variable s, and $|j>$ is a vibrational eigenstate with eigenvalue ϵ_j. All these computations were performed by the DiNa package.[36]

Solvent effects were evaluated by a modified version of the Gaussian-94 package including a new effective implementation of the polarizable continuum model (PCM).[37,38] In this model, the molecular free energy in solution (G_{solv}) is partitioned into four contributions:[39]

$$G_{\text{solv}} = G_{\text{el}} + G_{\text{cav}} + G_{\text{dis}} + G_{\text{rep}} \qquad (5)$$

The first term, referred to as the electrostatic solute−solvent interaction, is usually the most important, especially for polar or charged solutes in solvents with high dielectric constant. Furthermore, this contribution enters the quantum mechanical Hamiltonian, thus modifying at the same time the solvation energy and the solute electron density. In PCM, powerful numerical techniques are used to solve, in an essentially exact way, the resulting electrostatic problem and to compute electrostatic free energies together with the corresponding analytical gradients.[37,38]

The last three terms of eq 5 are related to the work needed to build the cavity in the solvent (cavitation free energy) and to the solute−solvent dispersion and repulsion interactions. Classical models are usually employed to compute these contributions together with their derivatives with respect to nuclear coordinates.[37,39] Although these terms do not modify the quantum mechanical Hamiltonian, they cannot be neglected in the evaluation of accurate solvation free energies and can also modify the optimized geometries in solution.

In the present study, a number of technical improvements have been employed for the first time. In particular, optimized structures and solvation energies have been computed by a cavity model that has been recently introduced and validated,[40] namely the united atoms model for Hartree−Fock computations (in short UAHF). Furthermore, geometry optimizations have been performed using the conductor-like polarizable continuum model (C-PCM),[41] which describes the solvent as a polarizable conductor instead of a polarizable dielectric like the original PCM (hereafter D-PCM). The C-PCM has been recently elaborated from the model originally proposed by Klamt and co-workers[42−44] and developed also by Truong and Stefanovich,[45,46] but mutuating the general algorithmic approach and the nonelectrostatic contributions from D-PCM. In its present form, C-PCM provides results very close to those obtained by D-PCM for high dielectric constant solvents, but it is significantly more effective in geometry optimizations, and it is less prone to numerical errors arising from the small part of the solute electron cloud lying outside the cavity (escaped charge effects).[47]

On the other hand, single-point computations have been performed also by D-PCM since, in this case, we can use a very refined and reliable charge compensation procedure that minimizes the escaped charge problem.[40] Moreover, in the UAHF model, hydrogen atoms are included in the same sphere of the heavy atom they are bonded to. Therefore, spectroscopic parameters have been computed also using more standard cavities formed by interlocking spheres centered on all atoms with radii proportional to van der Waals values (1.5, 1.5, 1.4, 1.2, and 1.0 Å for C, N, O, aliphatic, and acidic H, respectively).[22,24]

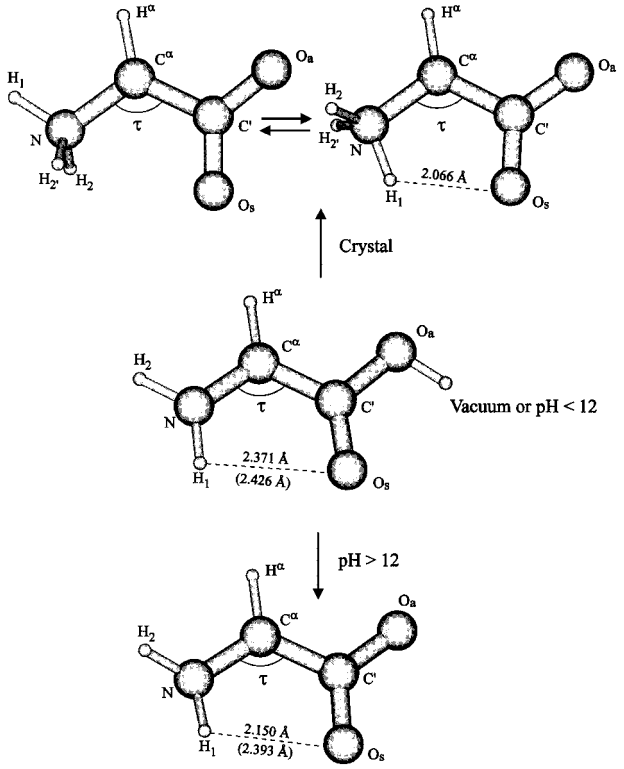

Figure 1. Structures and atom labeling of the glycine radicals considered in the present study. The intramolecular H bond distances computed in vacuo and in aqueous solution (in parentheses) are also reported.

3. Results and Discusison

Recent studies on the structures and stabilities of all the possible radicals derived from H atom extraction from glycine (N-centered, O-centered, and C-centered) concluded that C-centered radicals are significantly more stable.[8,14] Furthermore, cationic species never predominate in aqueous solution.[14,15] As a consequence, we will only consider the species whose general structures and atom labeling are shown in Figure 1.

The conformational behavior of these radicals is determined by torsions around the $C^{\alpha}-N$ (φ), $C^{\alpha}-C'$ (ψ), and, possibly,

(36) (a) Minichino, C.; Barone, V. *J. Chem. Phys.* **1994**, *100*, 3717. (b) Barone, V.; Minichino, C. *THEOCHEM* **1995**, *330*, 325.
(37) Cossi, M.; Barone, V.; Cammi, R.; Tomasi, J. *Chem. Phys. Lett.* **1996**, *255*, 327.
(38) Barone, V.; Cossi, M.; Tomasi, J. *J. Comput. Chem*. **1998**, *19*, 407.
(39) Tomasi, J.; Persico, M. *Chem. Rev.* **1994**, *94*, 2027.
(40) Barone, V.; Cossi, M.; Tomasi, J. *J. Chem. Phys.* **1997**, *107*, 3210.
(41) Barone, V.; Cossi, M. *J. Phys. Chem.* **1998**, *102*, 1995.
(42) Klamt, A.; Schüürmann, G. *J. Chem. Soc., Perkin Trans. 2* **1993**, 799.
(43) Andzelm, J.; Kölmel, C.; Klamt, A. *J. Chem. Phys*. **1995**, *103*, 9312.
(44) Klamt, A.; Jonas, V. *J. Chem. Phys.* **1996**, *105*, 9972.
(45) Stefanovich, E. V.; Truong, T. N. *Chem. Phys. Lett*. **1996**, *225*, 327.
(46) Truong,, T. N.; Stefanovich, E. V. *J. Chem. Phys*. **1995**, *103*, 3709.
(47) Cossi, M.; Barone, V. *Chem. Phys. Lett*., submitted.

Table 1. Geometrical Parameters (Å and Deg) for the Zwitterionic Form of Glycine Radical (See Figure 1) (All the Computations Have Been Performed at the B3LYP/6-31+G(d,p) Level)

	conformer 1 in vacuo	conformer 1 in aq soln	conformer 2 in aq soln
NC^{α}	1.486	1.458	1.451
$C^{\alpha}C'$	1.500	1.481	1.482
CO_s	1.271	1.268	1.272
CO_a	1.245	1.264	1.262
$C^{\alpha}H^{\alpha}$	1.084	1.082	1.081
NH_1	1.023	1.026	1.037
NH_2	1.031	1.029	1.029
$NC^{\alpha}C'$	110.87	118.13	115.91
$C^{\alpha}C'O_s$	111.44	116.11	115.11
$C^{\alpha}CO_a$	115.78	115.80	116.76
$NC^{\alpha}H$	132.11	126.26	126.58
H_1NC^{α}	115.19	111.62	106.03
H_2NC^{α}	107.31	111.81	112.83
$H_2NC^{\alpha}C'$	54.42	59.00	119.68

$C'-O$ (ω) bonds. However, contrary to the parent amino acids,[48] energy minima are found only for planar or nearly planar arrangements of the whole molecule[12] except two aminic hydrogen atoms. This is due to the replacement of the sp^3 C^{α} atom of glycine by a nearly sp^2 radical center, which allows an effective electron delocalization. This induces, in turn, a strong resistance to any deformation destroying the planarity of the molecular backbone, which counterbalances the increased strength of intramolecular hydrogen bridges characterizing nonplanar conformations.[48]

These trends are well evidenced by a comparison between the structural parameters of glycine and of the corresponding neutral radical.[24,48] The only significant differences concern an increase of the $NC^{\alpha}C'$ (τ) angle and the decrease of the NC^{α} and $C^{\alpha}C'$ bond lengths. At the same time, the NH_2 moiety is significantly more planar in the radical than in the parent amino acid (the sum of valence angles around N is 353° in the radical versus 326° in glycine).

3.1. Zwitterionic Form. In Table 1, we report the geometrical parameters for the zwitterionic form of the glycine radical optimized in vacuo and in aqueous solution at the B3LYP/6-31+G(d,p) level. They are referred to the two conformers drawn in Figure 1, the former with H_1(N) and O_s in anti orientation and the latter with these atoms nearly eclipsed and engaged in an intramolecular hydrogen bond.

As previously found for the parent amino acid,[49,50] the zwitterionic form does not correspond to an energy minimum for the isolated molecule. In particular, geometry optimization of conformer 2 leads to the neutral form, whereas constrained optimization of conformer 1 enforcing C_s symmetry leads to a saddle point of order 2. On the other hand, the zwitterion is stabilized by environmental effects in aqueous solution, and conformer 2 becomes a local energy minimum according to PCM computations. In vacuo, the constrained zwitterion is less stable than the neutral form by 211 kJ mol^{-1} at the B3LYP/EPR2 level. Solvent effects strongly reduce the energy gap between protomeric forms, and conformer 2 becomes less stable than the neutral form by only 102.5 kJ mol^{-1} at the B3LYP/EPR2 level. However, contrary to the parent amino acid, the zwitterionic form of the radical never predominates in aqueous solution. This is in agreement with experimental results[14−16] and points out the remarkable role of the captodative effect discussed in the Introduction.

In Table 2, the isotropic hcc's computed for both conformers in vacuo and in aqueous solution are shown. Experimental results, obtained recording the ESR spectrum of the glycine radical in the solid state,[17] are listed too.

Since the experimental ESR spectrum unambiguously shows that in the solid state the three H(N) atoms are equivalent (probably due to tunneling),[17] only average values of hcc's on H(N) atoms will be considered. Both the geometry and the hcc's calculated in vacuo are in good agreement with the corresponding values obtained at the MP2 level in previous studies,[14,51] thus confirming the reliability of the B3LYP approach. Furthermore, the introduction of environmental effects does not modify the results obtained for the isolated radical, which are already in fair agreement with experiment.

Coming to vibrational averaging effects, we recall that, among low-frequency vibrations, only those involving out-of-plane distortions have a significant effect for π radicals. Therefore, the LAP was traced using the distinguished coordinate (DC) approach, in which all the other geometrical parameters are optimized at selected values of a suitable internal coordinate (here, the out-of-plane displacement of H^{α}). As already shown in previous studies,[51−53] the hcc's of H^{α} and especially of C^{α} are strongly influenced by out-of-plane motion at the radical center. The hcc of C^{α} increases rapidly with the out-of-plane displacement of H^{α}, and this is clearly related to a strong change in hybridization. At the same time, the hcc of H^{α} increases more smoothly in absolute value. The hcc's of other atoms are essentially insensitive to this out-of-plane motion. When these effects are taken into account (fourth column in Table 2), we obtain an improved agreement with experiment especially for C^{α}.

Thus, the magnetic properties of glycine radical in its zwitterionic form are scarcely affected by the crystalline environment, and ESR spectra for this system are well reproduced by dynamic computations for the isolated radical. In particular, the hcc of the α-hyrogen has a value close to that of typical aliphatic π-radicals.

3.2. Anionic Form. In Table 3, we report the geometrical parameters for both the energy minimum (first three columns) and the planar saddle point (fourth column) of the glycine anion radical optimized in vacuo at various levels of calculation.

Our results indicate an essentially planar structure except for a significant pyramidality of the aminic moiety ($H_1NC^{\alpha}C' = 12.8°$ and $H_2NC^{\alpha}C' = 139.5°$ in place of 0° and 180°) in the equilibrium structure. It is noteworthy that H^{α} and H(N) hydrogens are on opposite sides of the mean molecular plane, although the out-of-plane distortion of H^{α} ($H^{\alpha}C^{\alpha}NC' = 172.6°$ in place of 180°) is lower than that of H_1 and, especially of H_2. All the geometrical parameters except the out-of-plane angles are very similar for the planar saddle point governing the inversion of the radical.

We have next considered the "direct" solvent effect on hcc's, i.e., the effect of the solvent-induced polarization on the solute wave function, without allowing any relaxation of the geometry optimized in vacuo. The corresponding hcc values evaluated at the B3LYP/EPR-2 level are shown in Table 4.

It is noteworthy that none of the calculated hcc's is in agreement with the corresponding experimental value and that the direct solvent effect is relatively small. In particular, the values for the aminic hydrogens are very far from experimental

(48) Barone, V.; Adamo, C.; Lelj, F. *J. Chem. Phys*. **1995**, *102*, 364.
(49) Ding, Y.; Krogh-Jespersen, K. *Chem. Phys. Lett*. **1992**, *199*, 261.
(50) Yu, D.; Armstrong, D. A.; Rauk, A. *Can. J. Chem*. **1992**, *70*, 1762.
(51) Barone, V.; Adamo, C.; Grand, A.; Subra, R. *Chem. Phys. Lett*. **1995**, *242*, 351.
(52) Barone, V.; Subra, R. *J. Chem. Phys*. **1996**, *104*, 2630.
(53) Barone, V.; Adamo, C.; Brunel, Y.; Subra, R. *J. Chem. Phys*. **1996**, *105*, 3168.

Table 2. Isotropic hcc's (Gauss) for $H_3N^+CHCOO^-$ (See Figure 1) Computed at the B3LYP/EPR-2 Level Are Compared with Experimental Results from Ref 17

	conformer 1 in vacuo		conformer 1 in aq soln		conformer 2 in aq soln		exptl
	a_{eq}	$\langle a\rangle_{77}$	a_{eq}	$\langle a\rangle_{77}$	a_{eq}	$\langle a\rangle_{77}$	$\langle a\rangle_{77}$
N	−3.1	−3.2	−2.9	−3.0	−3.2	−3.3	−3.5
C^a	38.2	43.0	35.1	40.0	34.0	38.8	45.0
C′	−11.2	−10.8	−12.7	−12.4	−13.1	−12.7	
H^a	−23.7	−22.2	−22.8	−22.4	−21.5	−21.0	−23.6
$1/3(H_1 + 2H_2)$	17.9	17.7	18.9	18.7	18.6	18.4	16.6

Table 3. Geometrical Parameters (Å and Deg) for the Energy Minimum and the Planar Saddle Point (SP) of the Anionic Form of Glycine Radical in Vacuo and in Aqueous Solution

	in vacuo				in aqueous solution	
	energy minimum			SP	energy minimum	SP
	B3LYP[a]	MP2[a]	B3LYP[b]	B3LYP[a]	B3LYP[a]	B3LYP[a]
bond lengths						
$C^\alpha-N$	1.401	1.398	1.393	1.385	1.375	1.369
$C^\alpha-C'$	1.487	1.488	1.483	1.483	1.457	1.457
$C'-O_s$	1.278	1.283	1.270	1.279	1.283	1.282
$C'-O_a$	1.268	1.273	1.259	1.269	1.283	1.281
$C^\alpha-H^\alpha$	1.087	1.080	1.081	1.085	1.084	1.085
$N-H_1$	1.024	1.019	1.019	1.014	1.017	1.018
$N-H_2$	1.018	1.011	1.011	1.004	1.015	1.016
O_s-H_1	2.150		2.137		2.393	
bond angles						
$N-C^\alpha-C'$	118.39	118.08	118.27	117.51	121.17	120.80
$C^\alpha-C'-O_s$	114.96	114.47	114.87	114.98	117.54	117.66
$C^\alpha-C'-O_a$	116.90	116.65	116.96	117.03	117.74	117.54
$N-C^\alpha-H^\alpha$	118.43	118.75	118.84	118.93	117.70	117.61
$H1-N-C^\alpha$	106.98	107.01	107.41	113.75	115.03	118.55
$H2-N-C^\alpha$	116.06	115.50	116.84	124.08	119.20	122.49
dihedral angles						
$H^\alpha-C^\alpha-C'-O_s$	172.55	174.78	175.56	180.00	178.14	180.00
$H1-N-C^\alpha-C'$	12.79	13.00	11.70	0.00	15.20	0.00
$H2-N-C^\alpha-C'$	139.50	139.86	140.73	180.00	157.71	180.00
$N-C^\alpha-C'-O_s$	−6.70	−5.75	−5.46	0.00	−4.13	0.00
$N-C^\alpha-C'-O_a$	174.02	176.93	175.12	180.00	177.29	180.00

[a] 6-31+G(d,p) basis set. [b] 6-311+G(2df,2p) basis set.

Table 4. Isotropic hcc's (Gauss) and Energy Barrier Governing Inversion (ΔE in kJ mol^{-1}) of Glycine Anion Radical Computed Using Geometries Optimized in Vacuo (See Table 3)

	energy minimum			planar saddle point		
	B3LYP/EPR-2	MP2/CHIP	B3LYP/EPR-2+D-PCM	B3LYP/EPR-2	B3LYP/EPR-2+D-PCM	exptl[a]
$a(N)$	7.58	7.55	8.14	2.35	3.44	6.1
$a(C^a)$	24.14	20.44	19.74	21.61	15.86	
$a(C')$	−10.97	−10.23	−9.99	−10.30	−8.63	
$a(O_s)$	−0.62	−0.68	−0.78	−0.47	−0.75	
$a(O_a)$	−2.13	2.19	−2.37	−2.41	−2.69	
$a(H^a)$	−17.08	−18.96	−16.33	−18.04	−16.01	13.8
$a(H_1)$	−1.06	−1.25	−1.56	−6.59	−7.93	3.4
$a(H_2)$	20.63	16.81	18.75	−6.85	−8.45	2.9
ΔE				14.23	1.45	

[a] Absolute values from refs 15 and 16.

results, casting some doubts about the reliability of the computational model. Further support to the B3LYP results is given, however, by the very similar geometries and hcc's obtained at the MP2 level (cf. columns 1 and 2 in Tables 3 and 4). Also, extension of the basis set at the B3LYP level does not introduce significant geometrical modifications (cf. columns 1 and 3 in Table 3).

The computed hcc's become more consistent with experiment for the planar geometry, thus suggesting that vibrational averaging and indirect solvent effects (i.e., those related to structural rather than to direct electronic modifications induced by the solvent) can be very important in the present case.

In Table 3 (fifth and sixth column), the geometrical parameters of the glycine anion radical optimized in solution at the B3LYP/6-31+G(d,p) level are compared to the values obtained by optimizations in vacuo (first and fourth column) both for the energy minimum and for the planar saddle point.

In both cases, the presence of the solvent shortens both the $C^\alpha-N$ and $C^\alpha-C'$ bonds, whereas the $C'-O$ bonds become slightly longer, corresponding to an increased weight of ionic resonance structures in polar media; moreover, the length of the intramolecular hydrogen bond is markedly increased in aqueous solution (see Figure 1). The most significant result is, however, that in solution the equilibrium structure is closer to planarity, the effect being particularly significant for H_2, whose torsional angle is increased from 139.5° to 157.7°.

The effect of the solvent-induced geometry relaxation on the

Table 5. Isotropic hcc's (Gauss) and Energy Barrier Governing Inversion (ΔE in kJ mol^{-1}) of Glycine Anion Radical Computed Using Geometries Optimized in Aqueous Solution (See Table 3)

	energy minimum			planar saddle point			
	B3LYP/EPR-2	B3LYP/EPR-2+D-PCM[a]	MP2/CHIP+D-PCM[a]	B3LYP/EPR-2	B3LYP/EPR-2+D-PCM[a]	B3LYP/EPR-2+C−PCM[a]	exptl[b]
a(N)	6.42	6.14 (6.18)	6.10 (6.12)	2.28	3.53 (3.45)	3.53 (3.46)	6.1
a(C$^{\alpha}$)	21.19	14.85 (14.73)	10.83 (10.85)	20.14	13.47 (13.41)	13.61 (13.52)	
a(C′)	−11.23	−9.30 (−9.21)	−9.62 (−9.57)	−10.88	−8.81 (−8.71)	−8.85 (−8.70)	
a(O$_s$)	−0.76	−1.10 (−1.10)	−0.43 (−0.45)	−0.71	−1.16 (−1.14)	−1.32 (−1.36)	
a(O$_a$)	−2.68	−3.02 (−3.07)	−0.68 (−0.71)	−2.77	−3.14 (−3.20)	−2.89 (−2.90)	
a(H$^{\alpha}$)	−17.88	−15.64 (−15.59)	−15.60 (−15.58)	−17.66	−15.10 (−15.09)	−15.15 (−15.11)	13.8
a(H$_1$)	−0.56	−3.12 (−3.20)	−4.07 (−4.02)	−6.73	−8.26 (−8.13)	−8.30 (−8.18)	3.4
a(H$_2$)	4.02	−0.63 (−0.71)	−1.57 (−1.56)	−6.77	−8.41 (−8.36)	−8.50 (−8.39)	2.9
ΔE				7.68	2.04	1.99	

[a] Using Pauling radii and UAHF radii (in parentheses). [b] Absolute values from refs 15 and 16.

Table 6. Isotropic hcc's (Gauss) of Glycine Anion Radical Averaged over the Linear Synchronous Path Defined in the Text at 0 and 298 K

geometry wave function	vacuo vacuo		vacuo aqueous solution		aqueous solution vacuo		aqueous solution aqueous solution		
	0 K	298 K	0 K	298 K	0 K	298 K	0 K	298 K	exptl[a]
$\langle a(N)\rangle$	7.34	7.28	5.66	6.13	6.48	6.74	5.52	6.02	6.1
$\langle a(C^{\alpha})\rangle$	24.21	24.19	17.54	17.98	21.32	21.41	14.99	15.26	
$\langle a(H^{\alpha})\rangle$	−17.14	−17.15	−16.12	−16.17	−17.93	−17.96	−15.70	−15.82	13.8
$\langle a(H_1)\rangle$	−1.42	−1.47	−4.88	−4.25	−0.51	−0.12	−4.53	−3.61	3.4
$\langle a(H_2)\rangle$	20.51	20.25	3.34	6.34	4.63	5.39	−2.46	−0.86	2.9

[a] Absolute values from refs 15 and 16.

hcc's is illustrated in Table 5, where we report the values calculated upon geometry reoptimization in aqueous solution.

The most important changes involve the aminic hydrogens in the equilibrium conformation: the geometry optimized by PCM being more planar, the aminic hydrogens hcc's are much more similar to each other.

Although the results are already reasonable at this level, large amplitude vibrational motions, in particular internal rotations and out-of-plane bendings, may affect the ESR parameters significantly. In the present case, torsional motions are strongly hindered, so we considered the out of plane motion of hydrogens with respect to the molecular (N−C$^{\alpha}$−C′) plane. Since the energy difference between the pyramidal energy minimum and the planar saddle point is strongly reduced in going from vacuo to aqueous solution (from 14 to 2 kJ mol^{-1}), we can expect that the role of vibrational averaging increases in the same direction.

The planar saddle point provides a good reference for the selection of suitable LAP's due to complete separation between in-plane (A′) and out-of-plane (A″) vibrations. An analysis of the normal modes of this structure shows that the transition vector essentially corresponds to the in phase displacement of H_1 and H_2 atoms, while a second low-frequency vibration involves the H$^{\alpha}$ atom. As a consequence, we decided to build two separate LAP's for these two motions. In particular, the displacement of H$^{\alpha}$ was treated by the DC approach discussed above for the zwitterion radical (but always retaining a planar arrangement of H_1 and H_2 in order to avoid double counting), whereas the displacement of H_1 and H_2 was described by the linear synchronous path (LSP) connecting the energy minimum and the saddle point.[33] We recall that the LSP is obtained through variations of all the geometrical parameters proportional to their difference between the energy minimum and the saddle point. Since vibrational averaging along the DC path essentially modifies only the hcc on C$^{\alpha}$ (which is not experimentally known), it will not be discussed in the following. The hcc's averaged along the LSP are, instead, shown in Table 6. Note that the populations of the vibrational excited states remain quite low at moderate temperatures, so that the results at 0 and at 298 K are not very different.

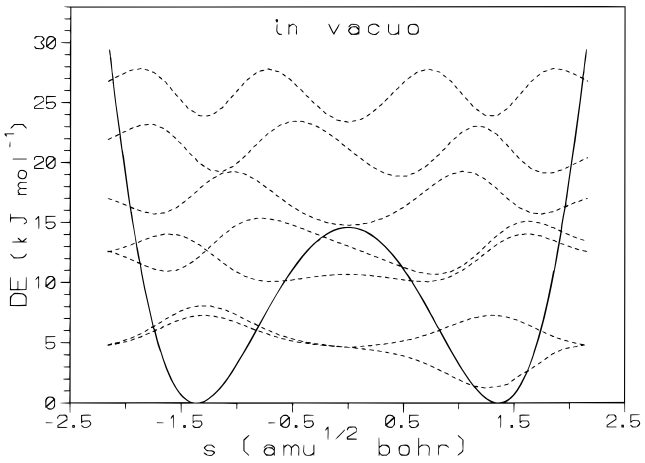

Figure 2. Energy potential and vibrational states for inversion of the glycine anion radical in vacuo from DiNa/B3LYP computations.

In vacuo, the anion radical is characterized by a significant inversion barrier and can be effectively treated as a system governed by a single-well potential unsymmetrically rising on both sides of the equilibrium structure (see Figure 2).

Since the potential rises less steeply, reducing the absolute value of the large amplitude coordinate, vibrational averaging leads to observables characteristic of structures with an aminic moiety slightly more planar than at the energy minimum. However, the effect is small since a high energy barrier necessarily implies a small vibrational amplitude around the equilibrium structure.

The situation is completely different for the anion radical in aqueous solution (see Figure 3), which is characterized by an inversion barrier lower than the zero-point energy for the out-of-plane vibration.

The ground vibrational wave function is now peaked at the planar structure, which, irrespective of being a saddle point, becomes the natural reference structure for evaluation of

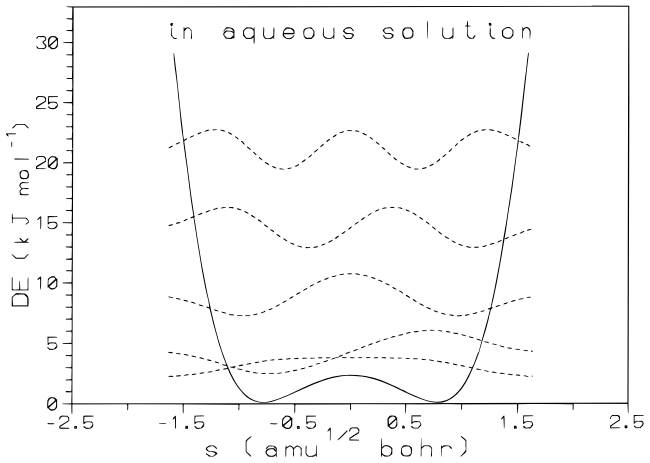

Figure 3. Energy potential and vibrational states for inversion of the glycine anion radical in aqueous solution from DiNa/PCM/B3LYP computations.

observables. Vibrational averaging then moves the coupling constants toward values that would have been obtained in a static description for a slightly pyramidal structure. The wave function of the vibrational ground state is significantly more delocalized than in the previous case (cf. Figures 2 and 3), so that averaging effects become more significant.

It is noteworthy that also for the neutral glycine radical solvent effects lead to a more planar equilibrium structure, but in that case the ground vibrational level is above the saddle point governing inversion already in vacuo.[24] As a consequence, indirect solvent effects (i.e., those related to structural rather than to direct electronic modifications) are quite negligible for the neutral radical, whereas they become of paramount importance for the anion radical.

To proceed further, we recall that hcc's can be decomposed in two contributions: a delocalization term, which is always positive (or null), and a spin polarization, or indirect contribution, which is positive at the radical center and generally negative for hydrogen atoms.[52−54]

In the planar structure, the delocalization effect vanishes since the singly occupied molecular orbital (SOMO) is a pure π orbital whose nodal plane coincides with the molecular plane (Figure 4).

Spin polarization, which is responsible for the strongly negative hcc of H^{α}, is roughly proportional[54] to the π spin density at C^{α}, so that delocalization of the SOMO reduces the hcc of H^{α}. Then Figure 4 clearly explains why the absolute value of the H^{α} hcc found for the anion radical is slightly higher than in the neutral radical and why both are significantly lower than in the zwitterionic form. Furthermore, the H^{α} hcc in the zwitterionic radical is close to the reference value of the methyl radical for which delocalization is, of course, impossible. Solvent effects enhance the delocalization along the backbone due to an increased weight of ionic resonance forms that involve double $N-C^{\alpha}$ or C^{α}-C′ bonds with the consequent reduction of the H^{α} hcc and of the pyramidality of the aminic moiety.

Spin polarization effects are nearly constant for H_1 and H_2, so that their hcc's are modified essentially by variations of the delocalization effect. These can be obtained by displacement of any atom above or below the nodal plane of the SOMO. Since the LSC essentially involves motion of H_2, we can expect a significant variation of the hcc of this atom. Figures 5 and 6 well illustrate this trend, which is quite similar in vacuo and in aqueous solution.

In conclusion, solvent effects lead from a strongly pyramidal to a quasiplanar species with a dramatic variation of the direct contribution to the H_2 hcc. At the same time, delocalization of the SOMO is increased with the consequent reduction of the π spin density on C^{α}, which, in turn, leads to a smaller spin polarization on H^{α}.

Considering the overwhelming role played by solvent effects, we have investigated the dependence of the results on different computational parameters (e.g., detailed shape of the molecular cavity, kind of wave function, etc.). The results shown in Table 5 clearly indicate that all the principal aspects discussed above (and actually also the numerical details) are very stable for different possible choices of the computational parameters. Note, however, that continuum solvent models employing simplified cavities (spheres or ellipsoids) and/or truncated multipolar expansions of the reaction field provide unreliable results.[24]

From another point of view, specific solute−solvent interactions, which are not explicitly taken into account in continuum models, could play a significant role especially for charged species. We have investigated this point by employing a mixed discrete-continuum approach in which the supermolecule formed by the solute plus the water molecules of its first solvation shell is immersed in the continuum polarizable medium. The number and the positions of the water molecules to be included in the supermolecule were determined by molecular dynamics simulations performed by the AMBER force field,[51] with rigid water geometries and keeping the glycine anion radical in the planar conformation optimized in vacuo at the B3LYP/6-31+G(d,p) level (see Table 3, fourth column). Consistent with the AMBER philosophy, the atomic charges of the glycine anion radical were obtained by fitting the quantum mechanical electrostatic potential.

Although thermodynamic and detailed structural parameters obtained by molecular mechanics approaches strongly depend on their parametrization,[56] general structural features appear well

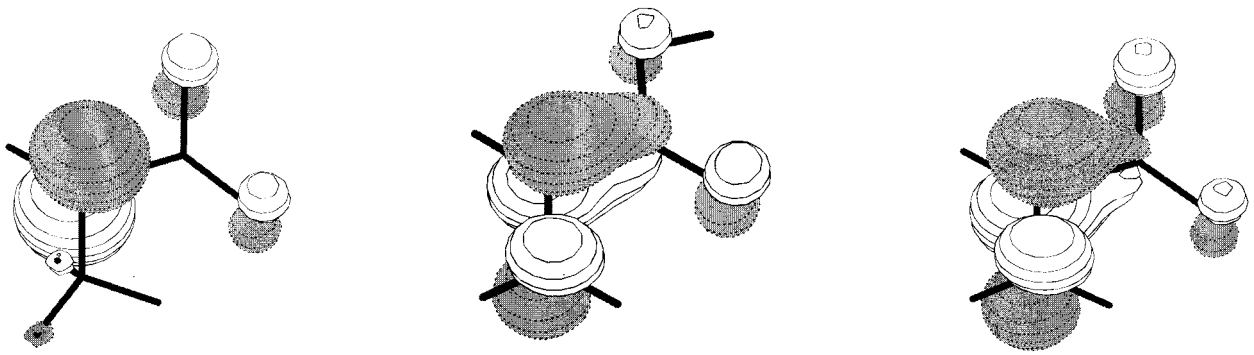

Figure 4. Singly occupied molecular orbital of zwitterionic, neutral, and anionic forms of the glycine radical according to B3LYP/6-31+G(d,p) computations.

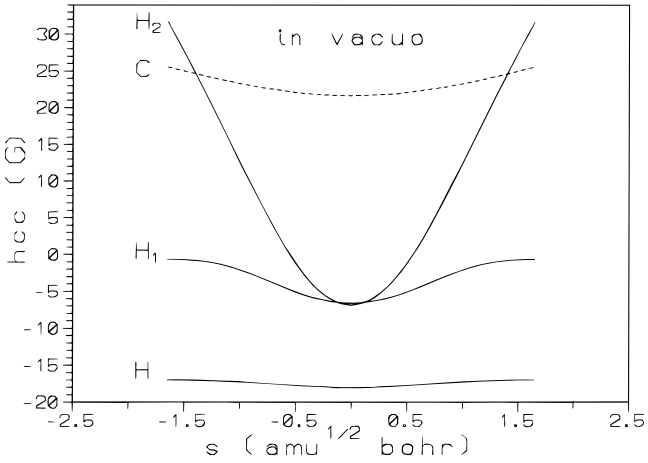

Figure 5. Dependence of isotropic hcc's computed at the B3LYP/EPR-2 level for the glycine anion radical in vacuo along the linear synchronous coordinate (LSC) defined in the text.

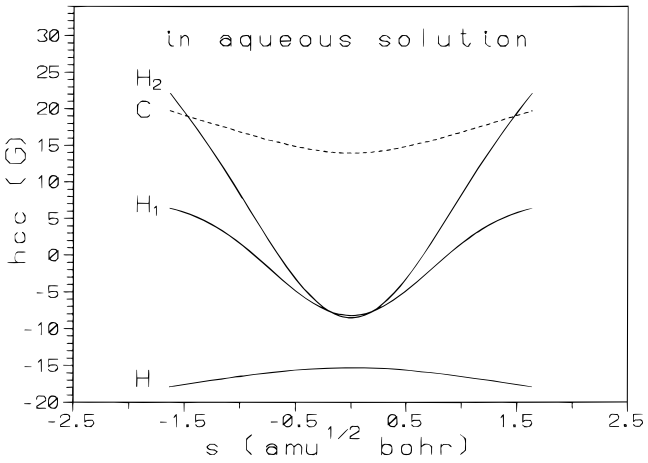

Figure 6. Dependence of isotropic hcc's computed at the B3LYP/EPR-2 level for the glycine anion radical in aqueous solution along the linear synchronous coordinate (LSC) defined in the text.

defined and only scarcely affected by different choices of the force field.[57] In particular, the AMBER force field correctly reproduces the stability order of hydrogen bridges between water molecules and aminic or carbonyl groups. Its only general shortcoming is an underestimation of hydrogen bond distances by about 0.2 Å with respect to experimental values.[57] This is rectified, however, by a successive reoptimization of the intermolecular parameters at the B3LYP level, which closely reproduces experimental values concerning both the strengths and the structural parameters of hydrogen bonds.[48,58]

The AMBER results clearly evidence three water molecules strongly bound around the COO^- moiety and a fourth water molecule more loosely bound to the H_2 aminic hydrogen. Actually, inclusion of this latter water molecule in the quantum mechanical supermolecule could be questionable from a purely energetic point of view, but several simulations by the AMBER force field invariably place a water molecule near the H_2 atom due to the combined effect of solute−solvent and solvent−solvent interactions. Unconstrained optimizations of the cluster containing just four water molecules at the B3LYP level moves this water molecule toward the charged carboxylic moiety (above or below the molecular plane). Since complete saturation of the carboxylic group by water molecules and further addition of a water molecule near H_2 is unpractical by quantum mechanical procedures, we resorted to a constrained optimization in which the O(W4)−H_2−N valence angle is frozen at the value issuing from AMBER computation. This leads to the structure shown in Figure 7.

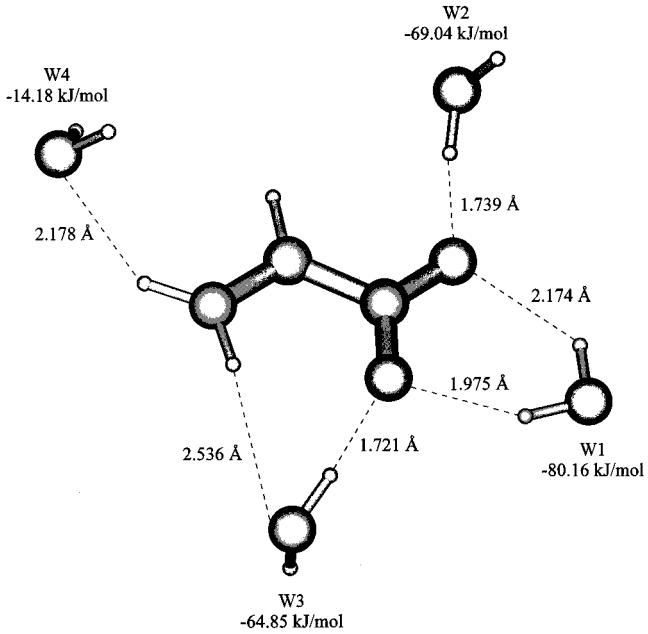

Figure 7. Structure and energetics of the adduct of glycine anion radical with four water molecules.

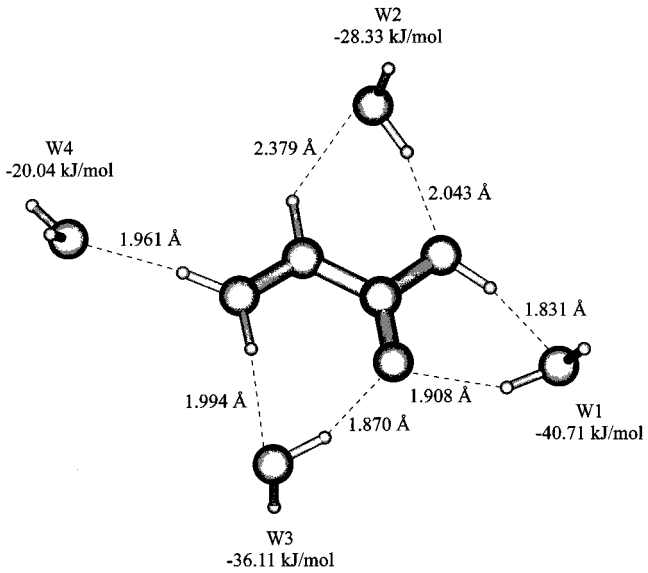

Figure 8. Structure and energetics of the adduct of glycine neutral radical with four water molecules.

The general features of this supermolecule are quite similar to those obtained by an analogous procedure for the neutral glycine radical[24] (see Figure 8), except for the much stronger interaction energies obtained for the charged species.

The ESR parameters were calculated at the B3LYP/EPR-2 level for systems including just one or all three strongly bound water molecules and for the same systems surrounded by the

(54) McConnell, H. M.; Chesnut, D. B. *J. Chem. Phys.* **1958**, *18*, 107.
(55) Cornell, W. D.; Cieplak, P.; Bayly, C. I.; Gould, I. R.; Merz, K. M., Jr.; Ferguson, D. M.; Sellmeyer, D. C.; Fox, T.; Caldwell, J. W.; Kollman, P. A. *J. Am. Chem. Soc.* **1995**, *117*, 5179.
(56) Amodeo, P.; Barone, V. *J. Am. Chem. Soc.* **1992**, *114*, 9085.
(57) Cristinziano, P. L.; Lelj, F.; Amodeo, P.; Barone, G.; Barone, V. *J. Chem. Soc., Faraday Trans. 1* **1989**, *85*, 621.
(58) Adamo, C.; Barone, V. In *Recent Advances in Density Functional Methods*; Chong, D. P., Ed.; World Scientific: Singapore, 1997; Part 2.

Table 7. Effect of the First Three Water Molecules of Figure 7 (See Text) on the hcc's (Gauss) of Glycine Anion Radical in Its Planar SP-Optimized in Vacuo

	water 1		water 2		water 3		3 H_2O	
	in vacuo	in aq soln	in vacuo	in aq soln	in vacuo	in aq soln	in vacuo	in aq soln
a(N)	2.47	3.50	2.43	3.49	2.57	3.61	2.80	3.71
a(C^{α})	20.86	15.50	20.58	15.24	20.48	14.98	18.64	13.77
a(C′)	−10.24	−8.57	−9.96	−8.26	−10.21	−8.36	−9.50	−7.61
a(O_s)	−0.52	−0.72	−1.01	−1.02	−0.26	−0.65	−0.84	−0.95
a(O_a)	−2.46	−2.87	−2.12	−2.61	−2.86	−2.99	−2.66	−3.08
a(H^{α})	−17.86	−15.87	−17.85	−15.80	−17.61	−15.60	−17.13	−15.11
a(H_1)	−6.76	−8.00	−6.71	−7.99	−6.86	−8.13	−7.14	−8.23
a(H_2)	−7.07	−8.53	−7.03	−8.53	−7.16	−8.66	−7.54	−8.81

Table 8. Effect of the Fourth Water Molecule of Figures 7 and 8 (See Text) on the hcc's (Gauss) of Glycine Anion Radical

	water 4[a]		water 4[b]		4 H_2O[a]		4 H_2O[b]	
	in vacuo	in aq soln	in vacuo	in aq soln	in vacuo	in aq soln	in vacuo	in aq soln
a(N)	2.56	3.42	2.56	3.48	3.01	3.92	3.03	4.02
a(C^{α})	21.06	15.77	20.52	15.30	18.05	12.76	17.40	12.10
a(C′)	−10.13	−8.62	−10.05	−8.46	−9.31	−7.14	−9.09	−6.86
a(O_s)	−0.46	−0.73	−0.50	−0.75	−0.82	−1.12	−0.87	−1.12
a(O_a)	−2.40	−2.71	−2.43	−2.74	−2.63	−3.01	−2.69	−3.08
a(H^{α})	−17.60	−15.98	−17.53	−15.75	−16.69	−14.57	−16.52	−14.24
a(H_1)	−6.86	−7.90	−6.86	−8.00	−7.44	−8.50	−7.46	−8.67
a(H_2)	−7.19	−8.40	−7.19	−8.41	−7.89	−9.05	−7.87	−9.10

[a] W4 placed as shown in Figure 7. [b] W4 placed as shown in Figure 8.

Table 9. Different Contributions to the hcc's (in Gauss) of Glycine Neutral and Anion Radicals Computed at the B3LYP/EPR-2 Level

	min vac	plan vac	Δ1st shell[a]	Δbulk[b]	Δgeo opt[c]	Δvib[d]	total	exptl[e]
				Anion Radical				
a(N)	7.58	2.35	0.66	0.91	0.09	2.49	6.50	6.1
a(H^{α})	−17.08	−18.04	1.35	2.12	0.91	−0.72	−14.18	13.78
a(H_1)	−1.06	−6.59	−0.85	−1.06	−0.33	4.65	−4.18	3.4
a(H_2)	20.63	−6.85	−1.04	−1.16	0.04	7.55	−1.46	2.9
				Neutral Radical (from Ref 24)				
a(N)	6.06	3.39	0.80	0.08	−0.01	1.63	5.81	6.38
a(H^{α})	−14.71	−14.40	2.59	0.24	0.17	−0.35	−11.74	11.77
a(H_1)	−5.31	−8.12	−0.82	−0.13	−0.01	2.51	−6.57	5.59
a(H_2)	−2.04	−8.51	−0.91	−0.11	0.03	3.83	−5.67	5.59

[a] Table 8, column 5 − Table 4, column 5. [b] Table 8, column 6 − Table 8, column 5. [c] Table 5, column 5 − Table 4, column 5. [d] Table 6, column 8 − Table 5, column 5. [e] Absolute values from refs 15 and 16.

continuum mimicking bulk solvent. The essential results of these computations are collected in Table 7.

We have considered separately the effect of the fourth water molecule (W4) obtaining the results collected in Table 8. For the purpose of illustration, we show only the results obtained for the orientation optimized for the neutral radical and for the structure obtained by the constrained optimization described above. They are representative of several other tests unambiguously showing that, while the presence of a water molecule near H_2 has a significant effect on the computed hcc's, its specific orientation is not very important.

From Tables 7 and 8, one can see that the water molecules have different effects on the various solute atoms, but the contribution of any solvent molecule cannot be neglected. It is also noteworthy that the spin transfer between the free radical and the solvent is very limited, so that the effect of specific interactions is rather to enhance the solute polarization through strong H-bonds with the molecules of the first solvation shell.

The role of specific (first solvation shell) and bulk (continuum) contributions to hcc shifts is comparable, so that neither the supermolecule nor a pure continuum model provide converged results. However, it remains remarkable that the PCM, though based on a simple and unstructured description of the solvent, is able to reproduce a significant part of the effect of the first solvation shell on the wave function even when H bonds are particularly important.

Our most accurate results for the different hcc's are obtained by adding to the values computed for the supermolecule with four water molecules immersed in the continuum the contributions due to geometry relaxation and to vibrational averaging. A dissection of the overall hcc's into these contributions is shown in Table 9 for both the neutral and anionic forms of the glycine radical.

The first remark deserved by these results is that the complete procedure suggested in the present study leads to good agreement with experimental values for all the isotropic hcc's. However, in our opinion, the most interesting aspect is that the role of the different contributions is significantly different for the neutral and charged species. In particular, vibrational and bulk solvent contributions are markedly more important for the anion radical. This is due to the greater flexibility (related to a less effective conjugation) and to the larger extension of the electronic cloud for the charged species. From Table 9, it would seem that geometry reoptimization in aqueous solution has a negligible effect. However, the partitioning of the overall values of hcc's between different contributions adopted in this table is somewhat misleading, since the largest effect of geometry reoptimization for the anion radical is hidden in the difference

between the first two columns (pyramidal vs planar strucures). Thus, none of the different contributions can be neglected for a reliable description: this points out, once again, the need for a comprehensive and reliable computational tool for the study of unstable species in solution.

4. Conclusion

In the present study, we have performed a detailed analysis of the structure and EPR features of the radicals derived from homolytic breaking of the $C^{\alpha}-H^{\alpha}$ bond of glycine in condensed phases.

From a methodological point of view, we have further validated a computational protocol associating a hybrid Hartree−Fock/density functional approach to a proper account both of vibrational averaging and of solvent effects. In particular, medium-size basis sets are sufficient to reproduce the effect of vibrational averaging and to provide reliable equilibrium values for structural, thermodynamic, and magnetic properties. Next, geometry relaxation in aqueous solution can be efficiently taken into account by PCM thanks to the implementation of analytical gradients nearly as effective as for in vacuo computations. At the same time, selection and first structural guesses of the supermolecule needed to properly take into account specific solvent effects can be reliably and efficiently obtained through molecular mechanics computations. Since all these computations are routinely feasible for quite large systems, the route seems paved for the fully a priori determination of structural and magnetic properties of radicals of biological interest in solution.

From a more specific point of view, we have unambiguously shown the close correlation between structure and ESR parameters of C-centered glycine radicals in aqueous solution. As a matter of fact, solvent effects, which are negligible for the zwitterionic form, have a significant effect for the neutral form and completely modify the ESR spectrum for the anionic form. In this latter case, the variation of the H_2 hcc is dramatic (from 20 to −1.5 G) and cannot be forecasted without a reliable and comprehensive computational protocol. At the same time, the equilibrium between different protomeric forms is tuned by intrinsic (e.g., captodative) and environmental (e.g., selective stabilization of charged species and/or resonance forms) effects. Thus, our study offers an internally consistent and very articulated scenario for the behavior of a typical amino acid radical in aqueous solution, which provides a direct link between macroscopic observables and the microscopic characteristics of a quite complex system.

Acknowledgment. We thank the Italian Research Council (CNR) for financial support to this research.

JA974232I